UNIVERSITY OF BATH

Citation for published version:
Weber, J, Wain, AJ, Piili, H, Matilainen, VP, Vuorema, A, Attard, GA & Marken, F 2016, 'Residual porosity of 3D-LAM-printed stainless-steel electrodes allows galvanic exchange platinisation', ChemElectroChem, vol. 3, no. 6, pp. 1020-1025. https://doi.org/10.1002/celc.201600098

DOI:
10.1002/celc.201600098

Publication date:
2016

Document Version
Peer reviewed version

Link to publication

University of Bath

REVISION

29th March 2016

Residual Porosity of 3D-LAM-Printed Stainless Steel Electrodes Allows Galvanic Exchange Platinisation

James Weber [1], Andrew J. Wain [2], Heidi Piili [3], Ville-Pekka Matilainen [3]
Anne Vuorema [4], Gary A. Attard [5], and Frank Marken *[1]

[1] *Department of Chemistry, University of Bath, Claverton Down, Bath BA2 7AY, UK*
[2] *National Physical Laboratory, Teddington, United Kingdom, TW11 0LW, UK*
[3] *Laser Processing Research Group, Lappeenranta University of Technology, Tuotantokatu 2, 53850 LPR Lappeenranta, Finland*
[4] *Lappeenranta University of Technology, Skinnarilankatu 34, 53850 Lappeenranta, Finland*
[5] *Department of Physics, The Oliver Lodge Laboratory, University of Liverpool, Oxford Street, Liverpool L69 7ZE, UK*

Abstract

Stainless steel rods were manufactured by laser additive manufacturing (LAM or "3D-printing") from a stainless steel (316L) powder precursor and then investigated and compared to conventional stainless steel in electrochemical experiments. The laser additive manufacturing method used in this study was based on "powder bed fusion" with in average 20-40 μm diameter particles are fused to give stainless steel rods of 3 mm diameter. In contrast to conventional bulk stainless steel (316L) electrodes, for 3D-printed electrodes small crevices in the surface provide residual porosity. Voltammetric features observed for the 3D-printed electrodes immersed in aqueous phosphate buffer are consistent with those for conventional bulk stainless steel (316L). Two chemically reversible surface processes were observed and tentatively attributed to Fe(II/III) phosphate and Cr(II/III) phosphate. Galvanic exchange is shown to allow improved platinum growth/adhesion onto the slightly porous 3D-printed stainless steel surface resulting in a mechanically robust and highly active porous platinum deposit with good catalytic activity toward methanol oxidation.

Graphical Abstract:

TOC Entry:

3D-printing of alloy and in particular stainless steel electrodes offers new prototyping technology, but also new opportunities for electrodes to be produced with new properties.

1. Introduction

The use of novel manufacturing techniques, such as laser additive manufacturing, LAM,[1,2] (also known as a type of 3D-printing[3]) can have a major impact on the rate and precision of complex fabrication processes such as device prototyping, small series production, as well as providing a tool for the synthesis of entirely novel composite materials. The technology allows the forging of complex 3D parts by melting and solidifying metallic, plastic, ceramic or composite powder materials layer-by-layer with a laser beam (see Figure 1 [4]). The quality and intricacy of parts manufactured using LAM technology is now on such a high level, that they can be used in various industrial applications as sophisticated functional components. For example, LAM processes have been used for the fabrication of complex channel networks for cooling, heating, and mixing, where similar structures are very expensive and time consuming to produce using conventional manufacturing methods.[5] Alloys and highly novel composites (e.g. metal-diamond) can be produced.[6] The scale of LAM technologies typically range from the production of individual prototypes up to a few hundred pieces.
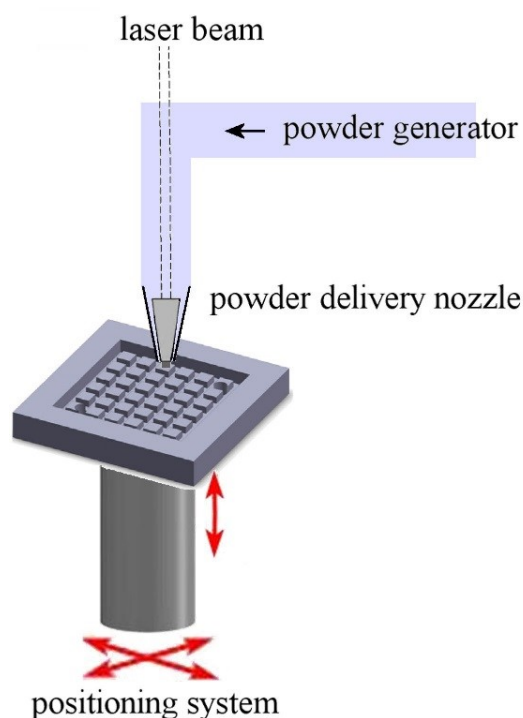
Figure 1. Schematic drawing of the laser additive manufacturing (LAM) process based on a powder flow (median diameter 31 µm) through a delivery nozzle with a laser (200 W continuous wave yttrium fibre laser source operating at 1070 nm wavelength) producing film deposits under nitrogen atmosphere.

Interest in 3D-printing techniques in chemistry[7] and in electrochemistry[8] is considerable and growing. Conventional lithography offers access to planar structures, for example with generator-collector electrode pattern,[9] but 3D-printing promises access to more complex structures with control over the third spatial dimension and printing of complete devices. Several types of 3D-printing technologies have emerged, for example based on ink jetting,[10] hot nozzle extrusion,[11] "bio-printing",[12] and laser-aided techniques.[13] In a recent study, Scotti et al.[14] created a stainless steel micro-fuel cell (MFC) made by LAM. The conclusion of the study was that the performance of the micro-fuel cell can scale with the lengthening/optimisation of the flow field, which is important in micro-fuel cell applications intended to power mobile devices. It was shown that structures with sub-

millimeter flow channels could be rapidly converted from computer-aided design to practical device. Despite the potential of application of LAM (and 3D-printing [15]) in the electrochemical sciences, there have been relatively few examples of its use in the fabrication of novel electrode materials.[16] Here, we investigate the electrochemical properties of 3D-printed stainless steel and propose its facile surface modification with a platinum catalyst via galvanic replacement. Crucially, the residual porosity in 3D-printed steel is shown to promote adhesion of the platinum deposit to the stainless steel substrate.

Stainless steel (316L) is composed of mainly Fe (62 wt%), Cr (17-19 wt%), (Ni 13-15 wt%), and smaller amounts of Mo, Mn, Si, and Cu. Stainless steel has found use as industrial substrate and counter electrode material[17] and has been investigated for applications in photo-electrochemical water splitting.[18] The surface of stainless steel itself is not typically catalytically active and therefore, in order to enhance reactivity of the surface, for example in fuel cell applications, the surface can be modified with catalytic materials such as platinum group metals. The interaction of such catalyst materials with stainless steel surfaces has been of interest, for example also in corrosion protection.[19] One convenient route to noble metal catalyst deposition is via galvanic replacement, which has been used previously to produce platinum nano-materials for fuel cell catalysis[20] as well as core-shell iron-rich Fe-Pt nanoparticles for heterogeneous catalysis.[21] The deposition process is driven by the formation of the more noble Pt, whilst dissolving Fe. The presence of metallic iron nanoparticles in carbon nanotubes has also been exploited for galvanic exchange deposition of Pt nano-catalysts.[22] The galvanic replacement methodology has been used in particular for Cu and Pb surfaces,[23] but there are no previous reports for galvanic exchange to

deposit catalytic platinum directly onto stainless steel (316L) electrode surfaces. It is shown here that the galvanic replacement offers a simple route to platinum-coated stainless steel (3D-printed) with good adhesion to the 3D-printed substrate due to residual porosity and with good reactivity towards the oxidation of methanol for potential application in methanol micro-fuel cell devices.

2. Experimental Details

2.1. Chemical Reagents

Methanol (MeOH, 99.8 %) and hexachloroplatinic(IV) acid (H_2PtCl_6) were obtained from Fisher Scientific and were used without further purification. Sulphuric acid (H_2SO_4, 95-98 %) and hydrochloric acid (HCl, stabilised at 1 M) were obtained from Sigma Aldrich UK and were used as received. Stainless steel (316L), nickel, and nickel-chromium 20-80 metal rods of 2 or 3 mm diameter were obtained from Advent UK. Purified water, with a resistivity of not less than 18 MΩ cm at 22°C, was used for the preparation of solutions. Argon gas (Ar) and nitrogen gas (N_2) were purchased from BOC UK (Pureshield).

2.2. Laser Additive Manufacturing of Stainless Steel Rods

The laser additive manufacturing (LAM) method employed here for stainless steel 316L has been reported in detail recently.[14] Figure 1 shows a schematic drawing with the principle components. Stainless steel powder (with typically 20-40 μm diameter particles) are supplied layer-by-layer via recoater and a 200 W laser (near-IR 1070 nm) is applied to melt material under an atmosphere of nitrogen. A custom-built

positioning system is employed to translate computer aided design structures into printed objects.

2.3. Instrumentation

A conventional three electrode cell set-up was employed for electrochemical measurements, using a KCl-saturated calomel reference (SCE) electrode, a Pt wire counter electrode and a 3D-printed stainless steel rod (316L grade) as the 3 mm diameter working electrode. Electrochemical experiments were carried out at room temperature, $22 \pm 2\ ^{\circ}C$, using an Ivium Compactstat (Ivium, Netherlands). All solutions were purged for 10 minutes using argon prior to performing electrochemical measurements.

2.4. Galvanic Exchange Deposition of Platinum on Stainless Steel

One end of the stainless steel rod was polished using P600 grade silicon carbide paper (Buehler) to produce a clean and slightly roughened surface, which was then rinsed with deionised water. Silicone sealant (Ambersil, Silicoset 150) was applied to the sides of the stainless steel rod to define a 3 mm diameter disc electrode. Galvanic exchange of platinum was achieved by immersion of the electrode into a solution of 2 mM hexachloroplatinic(IV) acid in 1 M HCl for 24 h at room temperature. After this treatment, the electrode was rinsed with deionised water and dried under N_2 gas. The process was repeated with a conventioinal 3 mm diameter 316L stainless steel rod (Advent UK) for comparison.

3. Results and Discussion

3.1. Characterisation of 3D-LAM-Printed Stainless Steel

The 3D-printed stainless steel electrode was first characterised by scanning electron microscopy (SEM, Figure 2). The electrode is compact/dense and generally similar in appearance to conventional stainless steel, with scratch features on the surface resulting from the polishing treatment. However, in contrast to conventional stainless steel some dark areas appear in the SEM image (Figure 2A), indicating minor crevices, likely formed due to the laser annealing process and resulting in residual porosity.
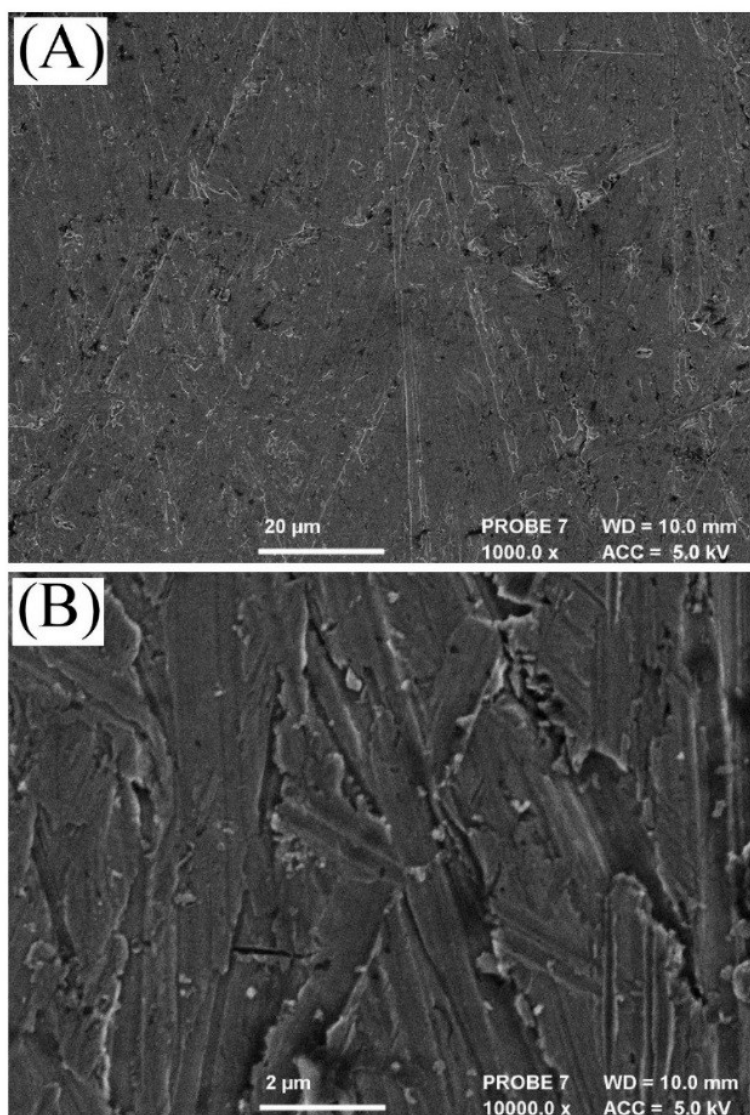
Figure 2. SEM images of 3D-printed stainless steel after polishing. Images recorded at (A) 1000 × and (B) 10000 × magnification.

Initial cyclic voltammetry experiments were performed using the 3 mm diameter 3D-printed stainless steel disc electrodes in argon-purged 0.1 M phosphate buffer solution at pH 7 (Figure 3). There are two prominent redox processes observed, both with oxidation and reduction peaks indicative of chemical reversibility.
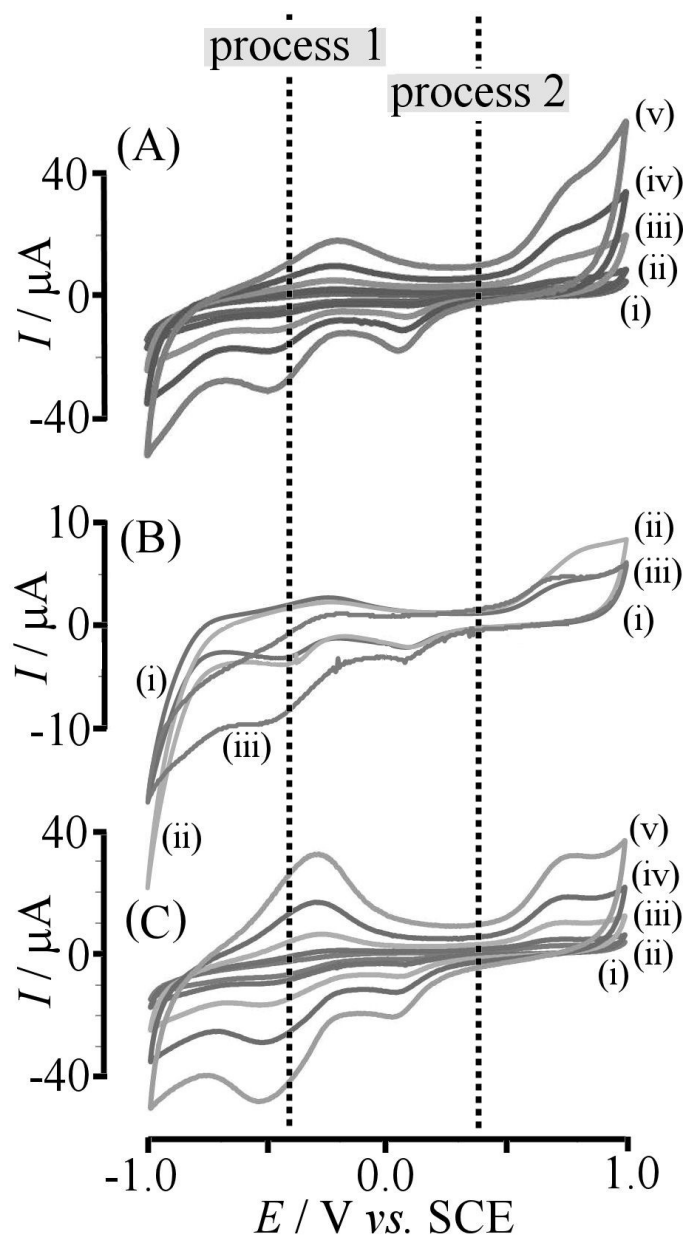
Figure 3. (A) Cyclic voltammograms (scan rate (i) 10, (ii) 20, (iii) 50, (iv) 100, and (v) 200 mVs^{-1}) for a bare 3 mm diameter 3D-printed stainless steel electrode immersed in 0.1 M phosphate buffer at pH 7 under argon. (B) As above, but (i) under argon, (ii) in ambient air, (iii) with 6 mM H_2O_2. (C) As above, with 6 mM H_2O_2 and with a scan rate of (i) 10, (ii) 20, (iii) 50, (iv) 100, and (v) 200 mVs^{-1}).

Process 1 is centred around -0.4 V vs. SCE (with a peak-to-peak separation of ca. 200 mV at scan rate 200 mVs^{-1}) can be identified (by comparison with literature data [24])

as a Fe(II)/Fe(III) type process associated with the iron phosphate material at the stainless steel – solution interface (equation 1).

Process 1:   Fe(II) $\rightleftharpoons$ Fe(III) + e$^-$ (1)
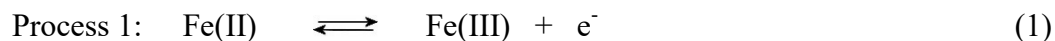
The second redox process centred around +0.4 V vs. SCE (with a much larger peak-to-peak separation of ca. 600 mV) is likely to be associated with Cr(II)/Cr(III) [25] (equation 2) rather than the presence of nickel phosphate material at the stainless steel | solution interface (see for example [26]).

Process 2:   Cr(II) $\rightleftharpoons$ Cr(III) + e$^-$ (2)
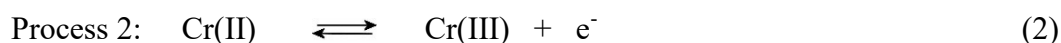
Additional experiments with nickel and nickel-chromium metal electrodes under the same experimental conditions were performed (not shown) to further confirm the tentative assignmnt as Cr(II/III) rather than Ni(II/III). For both redox couples peak current increased approximately linearly with scan rate consistent with surface immobilised redox processes (or with a thin film of redox active phosphate-based material). When comparing the voltammetric responses under argon and in the presence of ambient air (Figure 3Bi and 3Bii) it can be seen that the reduction of oxygen occurs only at very negative potentials well beyond the potential for the formation of Fe(II). However, when adding hydrogen peroxide the Fe(II)/Fe(III) redox system acts as a catalyst (Figure 3Biii), indicative of a two-electron reduction reaction of hydrogen peroxide at the surface of the stainless steel electrode to give water. This Fe(II)-catalytic reduction occurs at mildly negative potential before the reduction of oxygen. When investigating the effect of scan rate in the presence of 6

mM H_2O_2 (Figure 3C) the chemically reversible response for Fe(II)/Fe(III) appears enhanced compared to that for Cr(II)/Cr(III). When the same experiments were performed using a conventional 3 mm diameter stainless steel electrode, essentially identical voltammetric responses were obtained (not shown) confirming that, in terms of electrochemical performance, the 3D-printed stainless steel could be employed to replace conventional stainless steel.

3.2. Characterisation of 3D-Printed Stainless Steel after Galvanic Exchange Platinisation I: Surface Reactivity

The formation of catalytically active platinum on the 3D-printed stainless steel electrode surface occurs spontaneously under galvanic replacement conditions.[20,21] The iron component in stainless steel is the most electropositive metal component present, suggesting a reaction linking iron dissolution to platinum deposition (equation 3; note solution species are likely to form chloro complexes under these conditions).

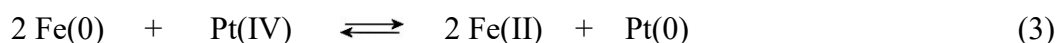$$2\,Fe(0) \quad + \quad Pt(IV) \quad \rightleftarrows \quad 2\,Fe(II) \quad + \quad Pt(0) \tag{3}$$

Figure 4A shows a typical scanning electron micrograph of platinum deposited using this approach, with nano-sized cauliflower-shaped platinum growth observed uniformly over the steel surface. The thickness of the film can be estimated from crevices (see Figure 4B) as being at least on the order of 10 μm after 24 h growth. Similar platinum films are obtained at conventional stainless steel surfaces, although with much poorer adhesion. When rinsing with water or tranferring into other

13

electrolyte media, the platinum film grown at the conventional steel usually delaminates and disconnects from the surface. In contrast, platinum films on 3D-printed stainless steel substrates are mechanically robust (presumably due to the residual prorosity in 3D-printed stainless steel) and can be used in electrochemical applications.
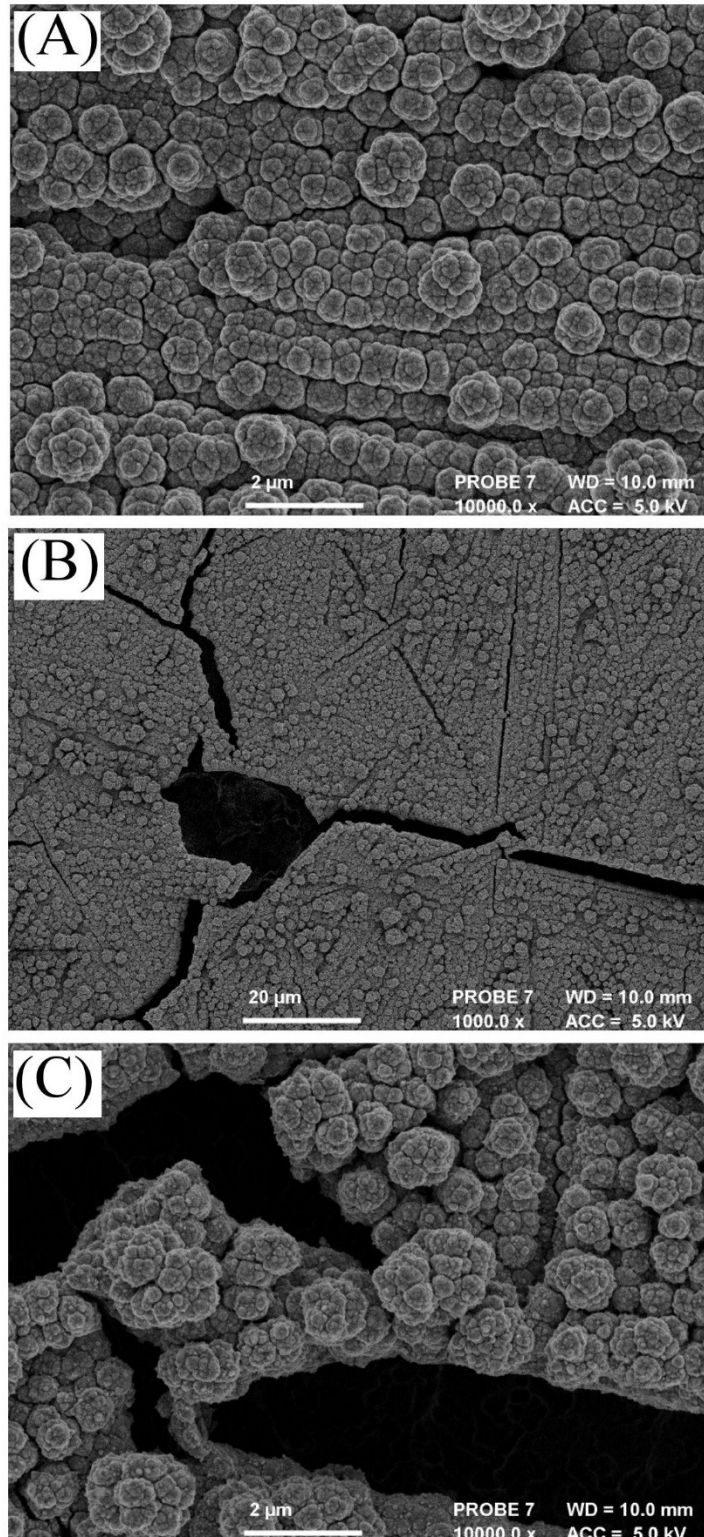
Figure 4. (A) Scanning electron optical image for pristine 3D-printed stainless steel after 24 h galvanic replacement with platinum. (B,C) Scanning electron optical images for "aged" 3D-printed stainless steel after galvanic replacement with platinum and 150 potential cycles in 0.5 M H_2SO_4. Images recorded at (B) 1000 × and (C) 10000 × magnification.

As expected, the presence of the platinum deposit has a significant effect on the electrochemical behaviour of the 3D-printed stainless steel surface. Voltammetry data in Figure 5 shows the characteristic platinum surface signals in 0.5 M H_2SO_4, where the platinum surface oxidation region (ca. 0.4 V to 1.1 V vs. SCE) and the hydrogen underpotential deposition region (ca. 0.1 V to -0.3 V vs. SCE) are clearly recognised.
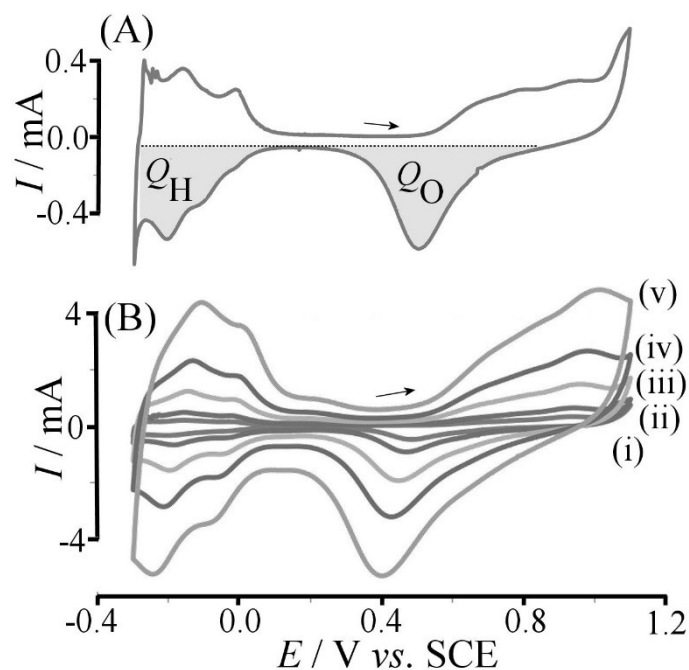

Figure 5. (A) Cyclic voltammogram (scan rate 20 mVs^{-1}) for a platinum coated 3 mm diameter 3D-printed stainless steel electrode immersed in argon-purged 0.5 M H_2SO_4 with oxide and hydrogen adsorption regions indicated. (B) As above, but with a scan rate of (i) 10, (ii) 20, (iii) 50, (iv) 100, and (v) 200 mVs^{-1}.

From the charge under the oxide region (Q_O = 0.15 mC) or the hydrogen region (Q_H = 0.11 mC) and using the corresponding conversion factors (here employing 0.21 mC

cm^{-2} [27,28]) it is possible to estimate the electrochemical surface area (ESA) for the active platinum as 0.52 cm^2. This suggests a roughness factor of 7.4, consistent with the appearance of the scanning electron micrographs. Comparison with data obtained with a 3 mm platinum disk electrode (see Table 1) demonstrates the similarity between galvanically exchanged and pure platinum.

Table 1. Measured electrochemical properties of platinised stainless steel electrode in aqueous 0.5 M H_2SO_4 (scan rate 20 mVs^{-1}). For comparison, data obtained for a 3 mm diameter Pt disk electrode under the same conditions are shown in the second row.

| Q_H: Charge under $H_{adsorption}$ / mC	Q_O: Charge under $(PtO_x/PtOH)_{desorption}$ / mC	Q_O/Q_H	Electrochemically Active Surface area / cm^2	Current Density for MeOH oxidation / mA cm^{-2}	Roughness Factor
0.11	0.15	1.4	0.52	13.4	7.4
0.08*	0.10*	1.3*	0.38*	0.08*	5.4*

* For comparison, data for a 3 mm diameter Pt disk electrode obtained under the same conditions.

When cycling the potential of the platinised stainless steel electrode for prolonged periods of time (150 continous cycles with scan rate 200 mVs^{-1}) a slow degradation of the platinum signal is observed (not shown) with ca. 20% loss of active area. The mechanism for this slow decay could be linked to changes at the underlying stainless steel electrode. Figures 4B,C show SEM images of the "aged" platinised surface after continuous cycling. It can be seen that stress arising in the platinum coating results in some cracking of the film, indicative of effects from some corrosion of stainless steel underneath the platinum film. Therefore, future applications of platinum-coated 3D-printed stainless steel electrodes will require mild conditions to minimise the rate of steel corrosion.

3.3. Characterisation of 3D-Printed Stainless Steel after Galvanic Exchange Platinisation II: Methanol Oxidation

The platinum deposit formed under galvanic replacement conditions can be employed in electrocatalysis. For example, a challenging test system relevant to fuel cell applications [29,30] is the oxidation of methanol to carbon dioxide (equation 4).

$$CH_3OH \ + \ H_2O \ \rightleftharpoons \ CO_2 \ + \ 6 \, H^+ \ + \ 6 \, e^- \tag{4}$$
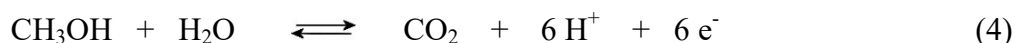
The potential beneficial role of iron "impurities" in methanol fuel cell systems has recently been highlighted by Antolini.[31] Figure 6A shows voltammetric data for a bare 3D-printed stainless steel electrode immersed in 0.5 M H_2SO_4 containing 0.2 M methanol. There is no obvious anodic signal associated with the methanol oxidation process, indicating that the unmodified steel electrode does not exhibit catalytic properties. However, in the presence of the platinum coating, significant anodic currents are obtained (Figure 6B). Peak features at 0.6 V vs. SCE (during the forward scan) and at 0.4 V vs. SCE (during the reverse scan) are associated with the methanol oxidation.[32] The fact that the anodic peak current is relatively independent of scan rate is characteristic for a catalytic process with surface-kinetic rate limiting processes. When polishing the electrode, platinum is removed and the majority of the catalytic response is removed. However, some platinum remains in crevices and for complete removal of platinum very vigorous and sustained polishing is required.
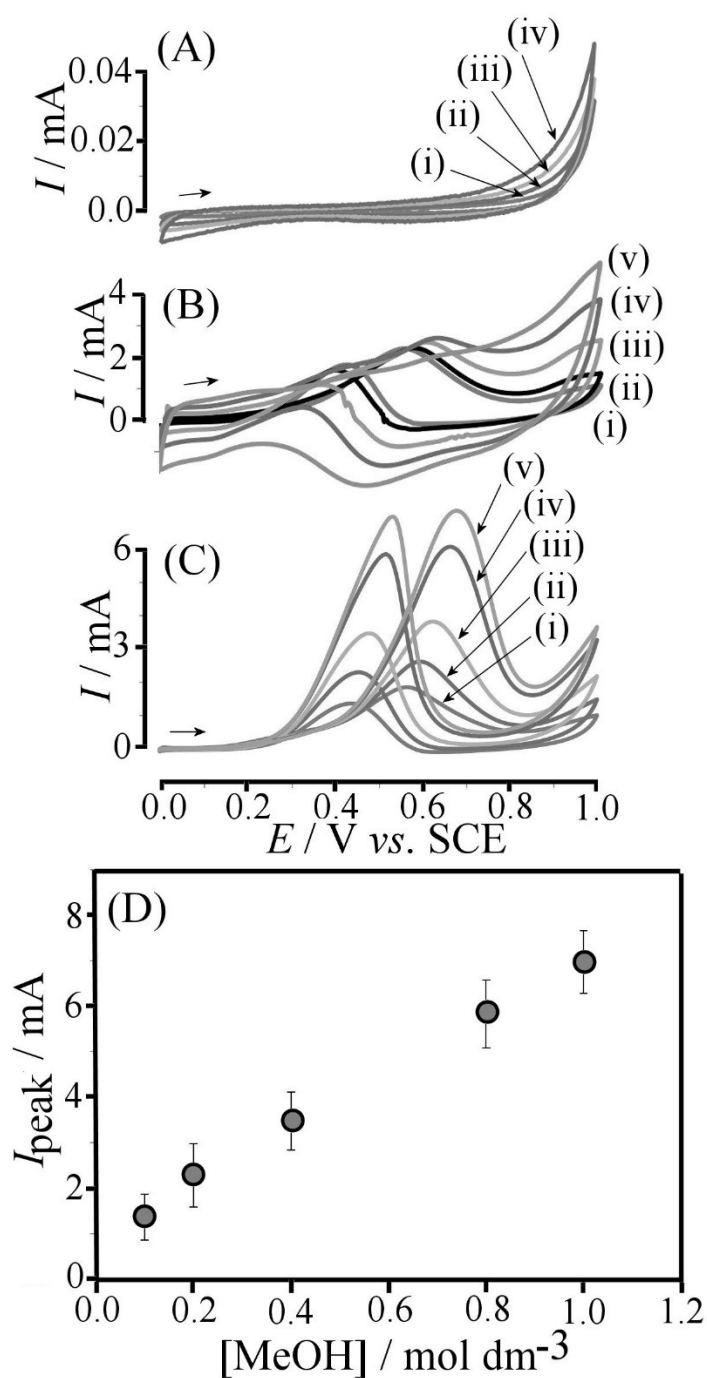
Figure 6. (A) Cyclic voltammogram (scan rate (i) 20, (ii) 50, (iii) 100, and (iv) 200 mVs^{-1}) for a bare 3 mm diameter 3D-printed stainless steel electrode immersed in 0.5 M H$_2$SO$_4$ containing 0.2 M methanol. (B) As above, but for a platinum-coated 3D-printed stainless steel electrode and scan rates of (i) 10, (ii) 20, (iii) 50, (iv) 100, and (v) 200 mVs^{-1}. (C) As above, but for platinum-coated steel at a scan rate of 20 mVs^{-1} and with (i) 0.1, (ii) 0.2, (iii) 0.4, (iv) 0.8, (v) 1.0 M methanol. (D) Plot of methanol oxidation peak current versus methanol concentration (error bars estimated).

19

When studying higher methanol concentrations, well-defined peak signals are observed (Figure 6C), and these are found to increase almost linearly with methanol concentration (Figure 6D). The absence of a peak current plateauing at higher methanol concentrations is indicative of a highly active catalyst. When normalised to the catalytic current density (by dividing the peak current by the electrochemically active surface area, *vide supra*), typical catalytic current densities (or specific activities) of 13.4 mA cm^{-2} are obtained for a 1 M methanol solution (see Figure 6D). This is relatively high and it compares well to typical values reported for good platinum alloy-based methanol oxidation catalysts [33] (under the same or similar experimental conditions). For bare platinum disc electrodes specific activity values an order of magnitude lower have been reported.[27] Data in Table 1 demonstrate a specific activity of only 0.08 mA cm^{-2} when employing a 3 mm diameter platinum electrode under the same conditions. We hypothesise that the good catalytic current in the 3D-printed stainless steel case is linked to the presence of "iron impurities" incorporated during corrosion of the underlying stainless steel electrode. The presence of iron as "dopant" in platinum nanoparticle catalysts has been reported to enhance catalytic activity for ethanol oxidation [34] and for methanol oxidation.[35] A high level of 50 atom% in FePt nanoparticles has been reported to enhance formic acid oxidation reaction.[36] It appears likely that the galvanic replacement reaction driven by iron dissolution is the cause of some iron incorporation, which then leads to enhancement of catalysis. Further and more systematic study of this phenomenon is needed in future.

4. Summary and Conclusion

The 3D-printing process allows stainless steel electrodes to be manufactured in complex shapes, for example as patterned surfaces or as compact cells, which can be employed for applications in energy generation or sensing. The 3D-printed stainless steel has been shown to be electrochemically active, consistent with conventional stainless steel (316L) without significant catalytic reactivity towards methanol. However, with galvanic replacement of platinum for iron at the stainless steel surface a highly active catalyst surface is obtained. The platinum layer is compact and relatively robust towards prolonged cycling in aqueous acidic solution. The platinum layer is also observed to be mechanically robust (when compared to similar films on conventional stainless steel) due to residual porosity in the 3D-printed steel material.

The reactivity of the platinum towards methanol oxidation is good when compared to platinum alloy catalysts and enhanced when compared to conventional platinum catalyst materials. This enhancement is likely to be associated with the presence of mainly iron metal impurities (originating from stainless steel during galvanic replacement). This observation will require further study and exploration for a wider range of catalytic processes.

The 3D-printing and galvanic deposition method described herein has the potential to allow construction of electrochemical devices without the need for complex manufacturing steps. By controlling residual porosity at the 3D-printed stainless steel surface and by adding new components for composite materials and alloys a wide

range of new electrode systems will be accessible. Hence, the use of 3D-printed stainless steel as a low cost electrode substrate could be commercially attractive.

Acknowledgements

References

[1]   I. Gibson, D.W. Rosen, B. Stucker, *Additive manufacturing technologies – Rapid prototyping to direct digital manufacturing*, Springer New York, 2010.

[2]   W. Steen, *Laser Material Processing*, London, Springer, 2003, p. 408.

[3]   S. Mellor, L. Hao, D. Zhang, *Internat. J. Production Economics*, **2014**, *149,* 194-201.

[4]   M. Manninen, H. Piili, A. Salminen, Proceedings for the 28th International Congress on Application of Lasers Electro-Optics (ICALEO), Orlando, USA, **2009**, 1458-1467.

[5]   B. Müller, R. Hund, R. Malek, N. Gerth, *Digital Product and Process Development Systems,* **2013**, *411*, 124-137.

[6]   A.B. Spierings, C. Leinenbach, C. Kenel, K. Wegener, *Rapid Prototyping J.*, **2015**, *21*, 130-136.

[7]   S.V. Ley, D.E. Fitzpatrick, R. Ingham, R.M. Myers, *Angew. Chem. Internat. Ed.,* **2015**, *54*, 3449-3464.

[8]   Z. Rymansaib, P. Iravani, E. Emslie, M. Medvidović-Kosanović, M. Sak-Bosnar, R. Verdejo, F. Marken, *Electroanalysis*, **2016,** DOI: 10.1002/elan.201600017.

[9]   A. Vuorema, H. Meadows, N. Bin Ibrahim, J. Del Campo, M. Cortina-Puig, M.Y. Vagin, A.A. Karyakin, M. Sillanpää, F. Marken, *Electroanalysis*, **2010**, *22*, 2889-2896.

[10]   B.W. An, K. Kim, H. Lee, S.Y. Kim, Y. Shim, D.Y. Lee, J.Y. Song, J.U. Park, *Adv. Mater.*, **2015**, *27*, 4322-4328.

[11]   A. Bellini, S. Güçeri, M. Bertoldi, *ASME. J. Manuf. Sci. Eng.,* **2004**, *126*, 237-246.

[12]   S.V. Murphy, A. Atala, *Nature Biotechnol.,* **2014**, 32, 773-785.

[13]   L. Costa, R. Vilar, *Rapid Protoyping J.*, **2009**, *15*, 264-279.

[14]   G. Scotti, V. Matilainen, P. Kanninen, H. Piili, A. Salminen, T. Kallio, S. Franssila, *J. Power Sources*, **2014**, *272*, 356-361.

[15]   M.D. Symes, P.J. Kitson, J. Yan, C.J. Richmond, G.J. Cooper, R.W. Bowman, T. Vilbrandt, L. Cronin, *Nature Chem.,* **2012**, *4*, 349-354.

[16]   K. Sun, T.S. Wei, B.Y. Ahn, J.Y. Seo, S.J. Dillon, J.A. Lewis, *Adv. Mater.*, **2013**, *25*, 4539-4543.

[17]   G. Hashmi, K. Miettunen, T. Peltola, J. Halme, I. Asghar, K. Aitola, M. Toivola, P. Lund, *Renewable Sustainable Energy Rev.*, **2011**, *15*, 3717-3732.

[18]   J. Georgieva, E. Valova, S. Armyanov, N. Philippidis, I. Poulios, S. Sotiropoulos*, J. Hazard. Mater.,* **2012**, *211*, 30-46.

[19]   J.H. Potgieter*, J. Appl. Electrochem.*, **1991**, *21*, 471-482.

[20]   X.W. Zhou, Y.L. Gan, J.J. Du, D.N. Tian, R.H. Zhang, C.Y. Yang, Z.X. Dai, *J. Power Sources*, **2013,** *232*, 310-322.

[21]   K. Mori, N. Yoshioka, Y. Kondo, T. Takeuchi, H. Yamashita, *Green Chem*., **2009**, *11*, 1337-1342.

[22]   K. Shimizu, J.S. Wang, C.M. Wai*, J. Phys. Chem. A*, **2010**, *114*, 3956-3961.

[23]   S. Ambrozik, N. Dimitrov, *Electrochim. Acta*, **2015,** *169*, 248-255.

[24]   K.J. McKenzie, F. Marken, *Pure Appl. Chem*., **2001**, *73*, 1885-1894.

[25]   C.Y. Cummings, G.A. Attard, J.M. Mitchels, F. Marken, *Australien J. Chem*., **2012**, *65*, 65-71.

[26]   A. Mohammadi, A.B. Moghaddam, M. Kazemzad, R. Dinarvand, J. Badraghi, *Mater. Sci. Engineer. C-Biomim. Supramol. Systems*, **2009**, *29*, 1752-1758.

[27]   C.E. Hotchen, G.A. Attard, S.D. Bull, F. Marken, *Electrochim. Acta*, **2014**, *137,* 484-488.

[28]   T. Biegler, D.A.J. Rand, R. Woods, *J. Electroanal. Chem*., **1971**, *29*, 269-273.

[29]   L. Lin, Q. Zhu, A.W. Xu, *Progress Chem*., **2015**, *27*, 1147-1157.

[30]   P. Kumar, K. Dutta, S. Das, P.P. Kundu, *Internat. J. Energy Res*., **2014**, *38*, 1367-1390.

[31]   E. Antolini, *RSC Adv*., **2016**, *6*, 3307-3325.

[32]   E. Herrero, K. Franaszczuk, A. Wieckowski, *J. Phys. Chem*., **1994**, *98*, 5074-5083.

[33]   N.S. Porter, H. Wu, Z.W. Quan, J.Y. Fang, *Acc. Chem. Res*., **2013**, *46*, 1867-1877.

[34]   T.S. Almeida, A.R. Van Wassen, R.B. VanDover, A.R. de Andrade, H.D. Abruna, *J. Power Sources*, **2015**, *284*, 623-630.

[35]   R. Kannan, A.A. Silva, F.M. Cardoso, G. Gupta, Z. Aslam, S. Sharma, R. Steinberger-Wilckens, *RSC Adv.*, **2015**, *5*, 36993-36998.

[36]   W. Chen, J.M. Kim, S.H. Sun, S.W. Chen, *Langmuir*, **2007**, *23*, 11303-11310.